We note that the required number of terms of the series in (11) to attain a relative error of 10^{-4} varies from 2 to a maximum of 4, depending on the input values.

As an example, we show in Fig. 2 the dependence of the speed of sound in a two-phase medium on pressure, taking into account the compliance of the walls of the channel and the surface tension. The different curves refer to different initial values of the gas content for "industrial 20" oil. In the calculations $\sigma = 0.03$ N/m, $R_0 = 0.3$ μm (taken from the data of [2]), and the rest of the data were taken from [1]. The calculations were performed on the SM-4 computer.

NOTATION

φ, gas content; V, V_g, volume of the gas–liquid mixture and the undissolved gas, respectively; σ, surface tension; c, pressure wave propagation velocity; E, modulus of elasticity; ρ, density; E_0, A, empirical constants; n, polytropic index; V_b, volume of a bubble; m, number of bubbles; ε, relative error, in %; subscripts: ℓ, liquid; g, gas; 0, initial state.

LITERATURE CITED

1. M. V. Khazanov, "Mathematical model of the dynamics of a liquid in a channel with the inclusion of the effects of undissolved gas and the compliance of the walls of the channel," Izv. Vyssh. Uchebn. Zaved., Mashinostr., No. 11, 54-57 (1983).
2. T. M. Bashta, I. Z. Zaichenko, V. V. Ermakov, and E. M. Khaimovich, Hydraulic Controls [in Russian], Mashinostroenie, Moscow (1969).

TIME-OF-FLIGHT MASS-SPECTROMETER WITH DUST-IMPACT ION SOURCE

S. B. Zhitenev, N. A. Inogamov, and A. B. Konstantinov

UDC 533.6.011.72:533.95+621.384.8

The processes occurring in a dust-impact mass analyzer, the ion source in which a plasmoid is formed in the impact of a high-velocity dust particle on the anode of the device, are studied.

1. A dust-impact mass analyzer (DIMA) is a combination of a time-of-flight mass spectrometer with a dust-impact ion source (see Fig. 1; a detailed diagram is presented in [1]). The device was developed in connection with the VEGA and Jotto expeditions to Haley's Comet [2]. The source of high-velocity particles is the dust cloud around the comet, moving toward the VEGA space probe with a velocity of $\mathbf{v}_0 = 78$ km/sec. The scientific goal of the project is the determination of the chemical and isotopic compositions of the comet material, which is important for the theory of evolution of the solar system. The device can also be used for mass-spectrometric analysis under terrestrial conditions [3].

The theory reveals two basic drawbacks of the device. The first one is the drop in the throughput capacity C of the device in the case of dust particles with low density ρ_d and mass M, where $C = N_C/N$. The question of the magnitude of C in the case of small dust particles is important, since for small N_C the limited sensitivity of the collector can cause the mass spectrum to be lost.

The drop in C is determined by the fact that the plasmoid formed in an oblique collision of the dust particle with the anode (see Fig. 1) moves at some angle to the normal, and as a result most of the ions fly past the collector. The problem of determining C involves the calculation of the angular distributions. This work is concerned with the problems arising here.

L. D. Landau Institute of Theoretical Physics, Academy of Sciences of the USSR, Moscow. Institute of Solid-State Physics, Academy of Sciences of the USSR, Chernogolovka.

Translated from Inzhenerno-Fizicheskii Zhurnal, Vol. 50, No. 5, pp. 751-760, May, 1986. Original article submitted February 18, 1985.

0022-0841/86/5005-0518$12.50

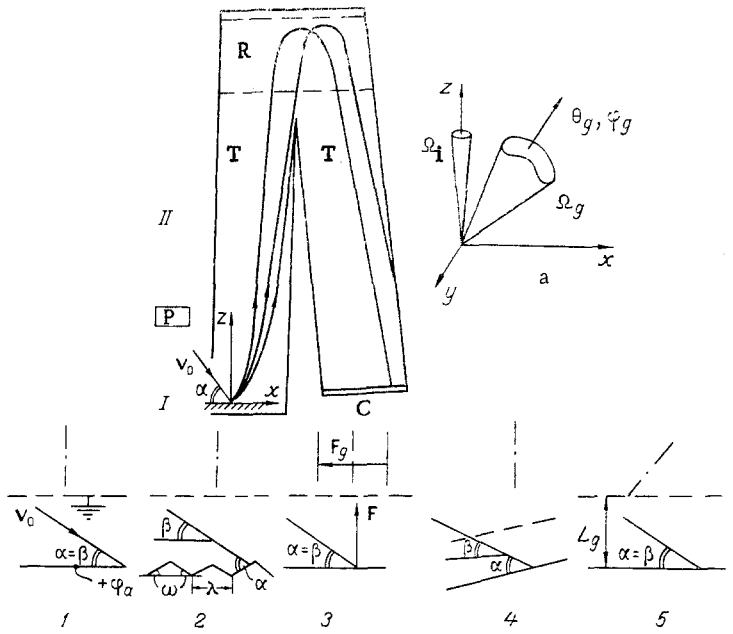

Fig. 1. Diagram of the DIMA device: block I is the ionization-accelerating chamber: 1-5) variants of block I; the dot–dash straight line corresponds to the axis of the input tube; block II: T) tubes; R) reflector; C) collector; P) photocell.

The second drawback of the device is the drop in the resolution $p = t_T/\Delta t$ in the case of large particles because of effects associated with the screening of the plasmoid by the electrostatic self-consistent field of the space charge (see [4]).

Two types of problems arise in connection with the use of DIMA: improvement of the device (optimization problems) and interpretation of the mass spectra (calibration problems).

The improvement of the device must proceed along two relatively independent paths: increasing the throughput capacity C in the case of small dust particles and increasing the resolution in the case of large dust particles. In this work we study the questions linked with increasing the value of C by controlling the direction of emergence of the plasmoid.

A great deal of experimental work has now been carried out on the solution of the problems of optimization and calibration of the device. The experiments were performed on a van de Graaf accelerator with a voltage of up to 2 mV [5, 6].

The acceleration of condensed particles up to high velocities $\mathbf{v}_0 \cong 10^2$ km/sec is a very difficult technical problem [7]. Record high velocities of $v_0 = 112$ km/sec can be achieved on a van de Graaf accelerator for submicron-size particles [8].

Unfortunately, the experiments were performed with dust particles consisting of heavy metals with $\rho_d > 8$ g/cm^3, velocities of the order of 10^2 km/sec can rarely be achieved, and the reproducibility of the results is poor. Nevertheless, in order to simulate accurately the conditions existing in experiments in space, a correspondence is required not only with regard to $\mathbf{v}_0$ and M, but also with regard to the density ρ_d. We note that the density of the comet dust grains $\rho_d = 0.8$-3 g/cm^3 [9] is several times lower than the density of the dust grains used in the experiment.

2. Structure of the Apparatus. The apparatus consisted of two main blocks. Block I is an ionization-acceleration chamber (IAC), consisting of a positive electrode (anode, Fig. 1, I) and a grid which accelerates the ions. Variants 2-5 are intended for obtaining higher values of C than can be achieved with variant 1. In variants 3-5 this is achieved via the component of the field perpendicular to the axis of the input tube (this axis is shown by the dot–dashed straight line in Fig. 1). Variant 2 with the fluted anode was proposed by R. Z. Sagdeev and variant 4 with the wedge-shaped arrangement of the electrodes was proposed by J. L. Berto. The variants 1 and 2 are of greatest interest for space experiments being planned [2]. In this paper we shall study primarily variant 1.

Block II consists of the flight tubes, reflector, and collector (Fig. 1). The main element is the collector. To increase $p = t_T/\Delta t$, the collector must have a small area and be

placed a large distance away. The much smaller dimensions of block I than those of block II enable working with the distribution of the velocities of the ion $\mathbf{w}$, measured in the laboratory coordinate system, in order to describe the motion of the ions in block I. We are interested in the ion distribution at the "inlet" and "outlet" of the accelerating gap of the IAC, which we denote by $f(\mathbf{w})$ and $f_g(\mathbf{w})$, respectively:

$$f(\mathbf{w}) = \partial^3 M / M \partial w_x \partial w_y \partial w_z, \tag{1}$$

$$f_g(\mathbf{w}) = \partial^3 N / N \partial w_x \partial w_y \partial w_z. \tag{2}$$

The function $f(\mathbf{w})$ coincides with the mass distribution of the dust particles over velocities in inertial flight (see Sec. 3). In calculating $f(\mathbf{w})$ the accelerating field $\mathbf{F}$ can be neglected. The function $f_g(\mathbf{w})$ gives the distribution of ions behind the grid up to the moment when all ions from the dust-grain material have flown behind the grid.

We denote by Ω_c the solid angle under which the collector is "visible" from the outlet of block I (see Fig. 1a). Because of the smallness of the collector and its remote position, the angle Ω_c is small: $\Omega_c/4\pi = \alpha_c^2/4\pi = 6 \cdot 10^{-5}$, where $\alpha_c = r_c/2L_T$.

In an oblique collision, the part of the initial component of the momentum of the expanding material of the dust grain parallel to the plane of the anode is conserved. In variants 1 and 2 this component is perpendicular to the field $\mathbf{F}$ and is therefore conserved, which produces an asymmetry in $f_g(\mathbf{w})$ relative to the z axis.

We denote by

$$g_g(\Theta, \varphi) = \partial^2 N / N \partial\Theta \partial\varphi \tag{3}$$

the post-grid angular distribution, calculated up to the moment when all dust grains have left the IAC. Here the angles Θ, φ are measured from the z and x axes, respectively, and the x, z plane passes through the vectors $\mathbf{F}$ and $\mathbf{v}_0$. Let Θ_g, φ_g be values of Θ, φ, such that $g_g(\Theta, \varphi)$ assumes its maximum value. We denote by Ω_g the solid angle containing the velocity vectors of the ions which have moved behind the grid of the IAC. It is clear that C is determined by the region of intersection of the angles Ω_c and Ω_g (Fig. 1a). The ratio

$$K = g_g(\Theta, \varphi)/g_g(\Theta_g, \varphi_g) \tag{4}$$

can serve as a quantitative measure of the asymmetry.

For qualitative evaluation we shall assume that the plasmoid is a uniform spherical cloud, which expands at a rate v_h and drifts as a whole across the field $\mathbf{F}$ with the velocity u_x. We shall calculate the velocities u_x and v_h:

$$u = (u_x, u_y, 0) = \int_{-\infty}^{\infty} \mathbf{w} f(\mathbf{w})\, d^3w, \quad v_h = \sqrt{\int_{-\infty}^{\infty} (\mathbf{w} - \mathbf{u})^2 f(\mathbf{w})\, d^3w}. \tag{5}$$

It is not difficult to see that when the volume charge is insignificant the ions which have moved behind the grid lie inside a cone whose axis forms an angle χ with the normal to the grid and has a flare angle of 2ψ, where

$$\psi = \frac{v_h}{v_g}, \quad \chi = \frac{u_x}{v_g} = \sqrt{2ze\frac{\varphi_a}{m_i}}. \tag{6}$$

The questions associated with the space charge are studied in Sec. 3 (see also [4]). With the exception of this section it is everywhere assumed that the self-consistent field is weak and does not affect the dynamics of the ions.

For typical values of the parameters u_x, v_h, $A/z \cong 10$, $\varphi_a = 3$ kV, we have $\Omega_c \ll \pi\psi^2$. Here A and z are the atomic weight and charge state of the ion, respectively. From here it follows that for $u_x > v_h$ the ions move outside the angle Ω_c and do not reach the collector.

The numerical experiments performed showed that the quantities K, u_x, and v_h depend primarily on the parameters α and $\mu = \rho_d/\rho_a$, where ρ_a is the initial density of the anode material. In the range of values of μ the functions $u_x(\mu, \alpha)$, $v_h(\mu, \alpha)$ with a fixed value of α depend monotonically on μ.

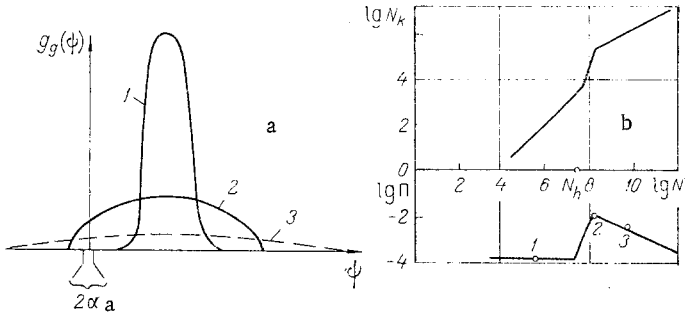

Fig. 2. Broadening of the post-grid angular distributions $g_g(\psi)$ [see (10)] because of the action of the SEF (a) and of the dependences $N_c(N)$ and $C(N)$ (b) in the case when the parameters (α, μ) lie in the region D of low values of the throughput capacity. Curves 1-3 correspond to the points 1-3 on curve C(N).

Remaining within the framework of a simple model of a spherical cloud with a sharp boundary, the dependence of K and therefore of C also on α and μ can be represented in the following simplified manner. In the (α, μ) plane there exists a neighborhood of the point $\alpha = \mu = 0$ which we shall call the region D, where the functions $K(\alpha, \mu)$, $C(\alpha, \mu)$ vanish. Outside D we have $K(\alpha, \mu) \simeq 1$. Region D is bounded by the curve of the critical values of the parameter $\mu = \mu_c(\alpha)$, on which condition $u_x(\mu_c, \alpha) = v_h(\mu_c, \alpha)$ holds.

In reality, the functions $C(\alpha, \mu)$, $K(\alpha, \mu)$ are continuous functions of their arguments, and the curve of the critical values $\mu = \mu_c(\alpha)$ is a transitional strip bounding the region of values $K(\alpha, \mu) \ll 1$. The remarks made here clarify the qualitative nature of the dependence of C on α and μ.

3. Basic Physical Processes. The complete problem can be divided into a series of coupled subproblems: I) the gasdynamic interaction of the dust grain with the anode; II) hardening of the ion composition; III) action of the external electric field on the expanding plasmoid.

Problem I consists of calculating the asymptotic structure of the plasmoid consisting of the dust-particle material. The inertial expansion is established when the plasmoid expands to a size of $R > R_1 = (2\text{-}4)R_0$, where R_0 is the initial size of the dust grain. When $R \gg R_0$, it may be assumed that the expansion occurs from a point. In this case the function f(w) (1) is related to the density as follows: $f(w) = \rho(r, t)t^3/M$.

The goal of problem II is to calculate the hardened composition. For typical values $R_0 = 0.1\text{-}1$ μm and $v_0 = 80$ km/sec, the hardening occurs when the plasmoid expands to a size of $R > R_2 = (10\text{-}10^2)R_0$ [10, 11]. When $R > R_3$ (where R_3 is several times larger than R_2) a collisionless flow state is established [11].

In problem III the action of the field on the dynamics of the plasmoid is calculated. This effect becomes important with expansion up to

$$R > R_4 = R_h = E_h/zeF = (10^3 - 10^4)R_0, \tag{7}$$

where $E_h = m_i v_h^2/2$. For typical values of the parameters we have $R_h \cong 1$ mm and $R_h \ll L_g \cong 1$ cm, where L_g is the distance from the anode to the grid. When the plasmoid expands up to dimensions $\cong R_h$, the plasma cools substantially:

$$T_4 = T(R_4) = T_2(R_2/R_4)^2 \ll E_h, \tag{8}$$

where T_2 is usually some fraction of the single-ionization potential.

If the degree of hardened ionization is known, $\chi = N/N_0$, then problems I and III can be solved independently of problem II. Here N and N_0 are, respectively, the number of atoms in the dust grain and the number of hardened ions. For parameters which are typical in space experiments $\chi \cong 1$ [10, 11].

The self-consistent electric field (SEF), associated with the ion space charge, can play an important role in the solution of problem III [4]. The strength of SEF is determined by the number N. When $N < N_h = E_h^2/z^3e^3F$, the SEF has no effect on the dynamics of the ions. In

this case, the ions in the uniform field F move along parabolic trajectories, which enables calculating $f_g(w)$ directly from $f(w)$. For $N > N_h$, the SEF is substantial and N becomes an important parameter: $C = C(\alpha, \mu, N)$. We shall describe, relying on [4], the behavior of C in the transitional region $N \cong N_h$.

Let the parameters α and μ lie outside the region D. Then [4],

$$\Pi \equiv \Pi_h \simeq \alpha_c^2/\psi^2 \simeq \alpha_\kappa^2 ze\varphi_a/E_h, \quad N < N_h,$$
$$\Pi \simeq \Pi_h (N/N_h)^{-2/5} \simeq \alpha_c^2 L_g F^{3/5} (zeE_h)^{-1/5} N^{-2/5}, \quad N > N_h, \tag{9}$$

where φ_a is the accelerating voltage difference.

Let α and μ belong to D, where C is small. Then SEF increases C in the transitional region $N \cong N_h$ (see Fig. 2). This is determined by the fact that because of the appearance of the x component of the field associated with the SEF the angular distribution becomes wider; the degree of broadening increases with N. The post-grid angular distribution

$$g_g(\psi) = \partial N/N\partial\psi, \quad \psi = \operatorname{arctg}(w_x/w_z) \tag{10}$$

is restructured, in this case, in the manner shown in Fig. 2. For $u_x \geq v_h$ the restructuring of $C(N)$ with increasing N occurs rapidly in the sense that the value of N_2 at which $C(N)$ assumes its maximum value is of the order of N_h. When $N > N_2$, $C(N)$ is determined by formula (9).

4. Numerical Model of the DIMA. The throughput capacity is a function of the following parameters:

$$[\mu]; \quad [\beta, \omega, n_\Gamma, \{\Gamma\}]; \quad [\{\gamma\}]. \tag{11}$$

Parameters (11) are grouped by the brackets into the following three groups: inertial, geometric, and thermodynamic. The notation $\mu = \rho_d/\rho_\alpha$ and the angles β and ω are defined in Fig. 1 (variant 2), and the parameter $n_\Gamma = 2D_p$, $2D_\alpha$, 3D, which corresponds to planar, cylindrical, and three-dimensional geometries, respectively. $\{\Gamma\}$ and $\{\gamma\}$ are collections of parameters which determine, respectively, the shape (and orientation) of the dust grains and the equation of the thermodynamic state of the materials of the dust grain and of the anode.

In the case of the geometry $n_\Gamma = 2D_p$, the motion occurs in the x, z plane (see Fig. 1). In this case the functions $f(w)$, $f_g(w)$ depend only on the velocity components w_x and w_z. The post-grid angular distribution is given by the function $g_g(\psi)$ [see (10)].

Two-dimensional flow appears with a collision of a filamentary dust grain, whose axis is oriented perpendicular to the x, z axis and whose length ℓ exceeds severalfold $R_1 = (2\text{-}4)R_0$, characterizing the expansion of the cloud with which the inertial expansion of the dust grain is observed (see Sec. 3). Here R_0 is the characteristic size in the transverse section of the filament. In the case of a collision which produces an asymmetrical flow, the calculation must be carried out in the 3D geometry. We note that because of the wider angular distributions in the 3D geometry and in $2D_p$ geometry, the values C_h ($C_h \equiv C$ for $N < N_h$), obtained with $n_\Gamma = 2D_p$, are higher than the values of C_h with $n_\Gamma = 3D$. Calculations of the $n_\Gamma = 3D$ case were carried out with $\mu = 0$ and are applicable for $\mu \leq 0.01$. These calculations are based on the following devices. For $\mu = 0$, the penetration of the barrier can be neglected and the problem of the interaction of the dust grain with a rigid wall can be studied. An oblique collision with a rigid wall admits a decomposition into a normal impact with a velocity $v_0 \sin\alpha$ and drift of the cloud as a whole along the surface of the barrier with the velocity $v_0 \cos\alpha$. The normal impact was calculated in the $2D_\alpha$ geometry. The results of the calculations in the 3D geometry are presented in Figs. 3b and 4b and in the tables. Figure 3b shows the contour lines of the function $g_g(w_x, w_y)$, determined by the following formula:

$$g_g(w_x, w_y) = \partial^2 N/N\partial w_x \partial w_y = \int_{-\infty}^{\infty} f_g(w)\, dw_z. \tag{12}$$

The function $g_g(w_x, w_y)$ is invariant under the transformation $w_y \to -w_y$, so that only half the picture is shown in the figure.

The studies show that the dependence of C on the parameters μ, β, and ω is most important.

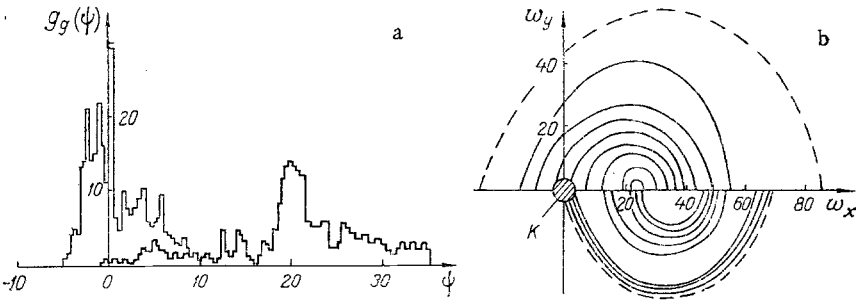

Fig. 3. Restructuring of the post-grid angular distributions with a variation of the fluting angle ω (as ω increases, the distributions shift toward the normal, which increases the number of ions hitting the collector); β = 30°, Γ = 1. ψ, deg; $g_g(\psi)$, %/deg; w_x, w_y, km/sec.

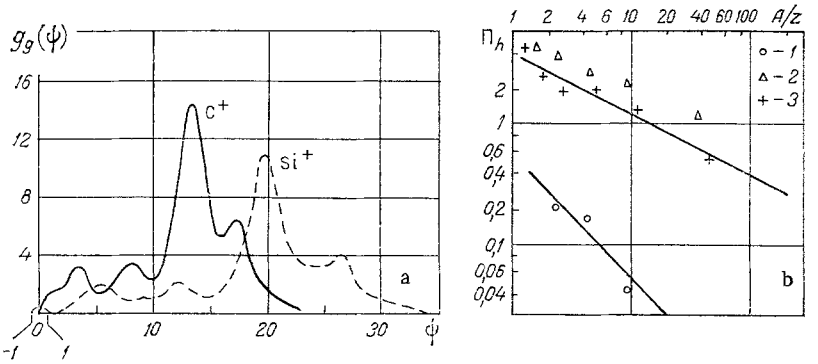

Fig. 4. Post-grid angular distributions of the ions C^+ and Si^+ (a) and the depencence of C_h on the parameter A/z (b). Each distribution is normalized to 100%: β = 30°, ω = 0°, Γ = 1, [C_h] = %; 1) μ = 0, $n\Gamma$ = 3D; 2) 0 and $2D_p$; 3) 0.11 and $2D_p$.

TABLE 1. Dependence of C_h on the Angles β and μ with ω = 0° and Γ = 1

β°	μ			
	0	0,037	0,11	0,37	0,5
30	1,1 | (0) / 0 | (0)	2±1	1,1±0,5	7	11
45	1,3 | (3,9·10⁻²) / 1,17 | (3,2·10⁻²)	1	14	—	—
60	2,66 | (5,4·10⁻²) / 2,40 | (5,8·10⁻²)	—	38	62	—
90	2,71 | [9,0·10⁻²] / 2,75 | [0,25]	—	81	—	—

The graphs and tables presented in this work were constructed for the following characteristic values of the parameters: φ_a = 3 kV, α_c = 1°, v_0 = 80 km/sec, A/z = 28, and A is the atomic weight.

In the columns of the tables corresponding to the value μ = 0 there are four numbers. The top pair of numbers correspond to calculations with the adiabatic index γ = 3 and the bottom pair corresponds to γ = 5/3. In these calculations we used the equation of state of a perfect gas. The parentheses enclose the results of calculations in the 3D geometry and the brackets enclose the results for the $2D_\alpha$ geometry. It was found that as the "rigidity" of

TABLE 2. Dependence of C on the Fluting Angle ω with $\beta = 30°$, $\Gamma = 1$, [C] = %

$\omega°$	μ		
	0	0,11	0,37
0	1,1 | (0) / 0 | (0)	1,1±0,5	—
15	1,25 | (0,042) / 0,89 | (0,078)	17	—
30	1,76 | (0,05) / 1,54 | (0,04)	24	19

the equation of state increases (i.e., the adiabatic index increases) the angular diagrams become broader. For an oblique collision this increases C; for a normal collision it decreases C. Calculations with $\mu \neq 0$ were carried out using the semiempirical equation of state of aluminum [12].

The dependence of C on μ and β with $\omega = 0°$ is shown in Table 1. As we can see, C increases with μ and β. As μ increases, the maximum of the distribution $g_g(\psi)$ shifts closer toward the normal, which increases C. The dependence of C on the shape and orientation of the dust grain was studied for the example of a dust grain with a rectangular cross section with height H and base d, parallel to the plane of the anode. The value of the parameter $\Gamma = H/d$ was varied in the calculations. For oblique collisions, C increased with the parameter Γ.

We shall study the question of the effect of the fluting of the surface of the anode on the throughput capacity (see Fig. 1, variant 2). Table 2 summarizes the corresponding results. The growth in C is caused by the increase in the region of intersection of the angles Ω_c and Ω_g, defined in Sec. 2, with increasing ω. The latter circumstance is determined by the fact that as the angle ω increases, the post-grid angular distribution shifts closer to the normal to the grid (see Fig. 3). The circle K here separates the region $\sqrt{w_x^2 + w_y^2} \leqq v_c = \alpha_c v_g$, containing the ions hitting the collector. As we can see, the best result is achieved with $\omega = 30°$.

We note that the spacing λ of the periodic fluted structure on the surface of the anode (see Fig. 1, variant 2) must satisfy the conditions $R_0 \ll \lambda < R_h$, where R_0 is the initial size of the dust grain; R_h is given in (7). The condition $\lambda < R_h$ must hold in order that the distortions of the electric field associated with the serrated structure be insignificant during the acceleration of the ions. We note that this condition is not necessary. The variant of the ionization-accelerating chamber with a nonuniform field in the accelerating gap, for example the scheme with a wedge-shaped arrangement of the electrodes (see Fig. 1, variant 4), is possible.

We shall study the case of a multicomponent plasma. The distribution f(w) in this case is the same for different ionic components, if the hardened plasmoid, as presumed here, has a spatially uniform ionic composition. We shall confine our attention to the case when the SEF does not affect the ion dynamics. The post-grid distribution $f_g(w)$ and, correspondingly, the values of C_h, are different for ionic components with different values of the parameter A/z. As A/z increases, the deflection of the corresponding plasmoid of ions from the normal to the grid increases and the solid angle Ω_g corresponding to these ions increases (Fig. 4a). As a result of this C_h decreases as A/z increases (Fig. 4b). It is not difficult to see that if the post-grid angular distributions are approximated by some distributions which are constant within the corresponding solid angles Ω_g, then in the cases $n_\Gamma = 2D_\alpha$, 3D we shall have $C \sim (A/z)^{-1}$ (the straight line in Fig. 4b) and $C_h \sim (A/z)^{-1/2}$ in the case $n_\Gamma = 2D_p$ (straight line 2 in Fig. 4b). Figure 4 is constructed in the following manner. Function f(w) is found from the gasdynamic numerical calculation and was assumed to be the same for ions with different values of A/z. The numerical calculation for Fig. 4a was carried out for the following values of the parameters: $\mu = 0.11$, $\beta = 30°$, $\omega = 0°$, $n_\Gamma = 2D_p$, $\Gamma = 1$. It was then assumed that the plasmoid consists of a mixture of different ions. A separate function $f_g(w)$ was calculated for each ionic component. An example of this calculation was shown in Fig. 4a. The points 1-3 in Fig. 4b were obtained by integrating over subintervals of the histograms of the post-grid angular distributions, analogous to those presented in Fig. 3a.

The values of C represent the ratio (in %) of the numbers of ions of a given type A/z hitting the collector to the total number of ions of this type in the hardened plasma of the dust grain material.

We note that the limit N_h of the region of values of N up to which the effect of the SEF on the ion dynamics of a given component can be neglected is different for different components. Calculations based on the perturbation theory give $N_{hm} = (m_m/m_b)^{2\cdot5}N_{hb}$, $N_{h\ell} = (m_\ell/m_b)^{2}\cdot N_{hb}$, where the index b refers to the base component, and the indices ℓ and m refer, respectively, to the light and heavy impurity ions ($m_\ell < m_b < m_m$). It was assumed that $z_\ell = z_b = z_m = z$. The quantity $N_{hb} = N_h$, where N_h is given by (8), if in (8) m_b is substituted for m. The perturbation theory is applicable when $N_\ell \leqslant N_b$, $N_m \ll N_b$, where N_ℓ, N_b, and N_m are, respectively, the number of hardened ℓ, b, and m ions in the plasmoid.

A complex of programs, including calculations of the gasdynamics of the interaction of the dust grains with the anode, the kinetics of ionization and recombination of the plasma, and the effect of the electric field on the dynamics of the plasmoid, was developed for studying the DIMA theoretically. The complex contains two gasdynamic codes: programs based on the large-particle method [13] and programs based on the particles-in-a-cell (PIC) method [14].

The PIC method was used to perform calculations of variants with $\mu \neq 0$. Special attention was devoted to obtaining an accurate resolution of the contact boundary between the materials of the dust grain and the anode. Variants with $\mu = 0$ in $n_\Gamma = 2D_p$, $2D_\alpha$, and 3D geometries were calculated by the large-particle method. These calculations cover the region of small values of the parameter $\mu \leq 0.01$. It should be emphasized that the calculation of C_h with $\mu = 0$ gives the lowest value of C_h that is possible for the given values of the parameters (β, ω, n_Γ, Γ). The spatial step in the calculations was equal to 1/7-1/20 of the size of the dust grain, and the grid consisted of 4-5 thousand nodes. When necessary, the grid was enlarged and the working field was adjusted.

NOTATION

v_0, velocity of the space probe relative to the dust cloud; C, throughput capacity of the device; N_c, number of ions from the dust grain entering the collector; M, mass of the dust grain; N, number of "hardened" ions of the dust grain; ρ_d, density of a dust grain; ρ_a, density of the anode (target); p, resolution of the device; t_T, flight time of the dust grain ion through the tubes in the device; Δt, width of the signal on the collector for a dust grain; w, velocity of the ion in the laboratory coordinate system; f(w), $f_g(w)$, velocity distribution functions of the ions at the starting and end points of the ionization-accelerating chamber; F, accelerating field; Ω_c, solid angle under which the collector is "visible" from the output of the block I; r_c, radius of the collector; L_T, total length of the flight tubes; Θ, φ, angular coordinates of the ion; $g_g(\Theta, \varphi)$, angular distribution of the ions behind the grid.

LITERATURE CITED

1. G. V. Lebedev and R. S. Churaev, "Ion-optical calculation of time-of-flight mass spectrometer," Preprint No. Pr-750, IKI, Academy of Sciences of the USSR (1982).
2. H. Fechtig, "Scientific objectivities of dust experiments on cometary fly-by missions in cometary exploration," in: Proceedings of the International Conference on Cometary Exploration, Budapest (1982), Vol. 2, p. 203.
3. P. K. D. Feigl, F. R. Krueger, and B. Schueler, "A simple technique of ion generation from organic solids by ultrashort electric pulses," Org. Mass Spectrosc., 18, No. 10, 442-443 (1983).
4. N. A. Inogamov, "Electrostatic screening by self-consistent volume charge and ion dynamics in a time-of-flight mass-spectrometer with a dust-impact ion source," Preprint Pr-950, IKI, Academy of Sciences of the USSR (1984).
5. H. Fechtig, H. Grün, and J. Kissel, "Laboratory simulation," in: Cosmic Dust, J. A. McDonnell (ed.), Wiley, New York (1978).
6. W. Knabe and F. R. Krueger, "Ion formation from alkali iodine solids by swift dust particle impact," Z. Naturforsch., 37a, No. 12, 1335-1340 (1982).
7. B. M. Manzon, "Acceleration of microparticles for controlled thermonuclear fusion," Usp. Fiz. Nauk, 134, No. 4, 611-640 (1983).

8. J. F. Friichtemicht and D. G. Becker, "Measurements of the ionization probability of Cu and LaB_6 simulated micrometeors," Astrophys. J., 166, No. 3, Pt. 1, 717-724 (1971).
9. J. M. Greenberg, "Laboratory dust experiments – Tracing the composition of cometary dust," in: Proceedings of the International Conference on Cometary Exploration, Vol. 2, Budapest (1982), p. 23.
10. S. Drapatz and K. W. Michel, "Theory of shock-wave ionization upon high-velocity impact of micrometeorites," Z. Naturforsch., 29a, 870 (1974).
11. Yu. G. Malama, "Numerical modeling of ionization phenomena in a high-velocity collision," Preprint Pr-725, IKI, Academy of Sciences of the USSR (1982).
12. A. V. Bushman and V. E. Fortov, "Models of the equation of state of materials," Usp. Fiz. Nauk, 140, No. 2, 177-232 (1983).
13. O. M. Belotserkovskii and Yu. M. Davydov, "Nonstationary method of 'large particles' for gasdynamic calculations," Zh. Vychisl. Mat. Mat. Fiz., 11, No. 1, 182-207 (1971).
14. M. W. Evans and F. H. Harlow, "The particle-in-cell method for hydrodynamic calculations," Rept. No. LA-2139, Los Alamos Scientific Laboratory (1957).

CROSS SECTION FOR THE INTERACTION OF SLOW NEUTRONS WITH CO_2 NEAR THE VAPORIZATION CRITICAL POINT

L. A. Bulavin and Yu. B. Mel'nichenko

UDC 539.125.52:536.44

The results of studies of the temperature dependence of the total cross section for the interaction of slow neutrons with CO_2 in a wide temperature range, including the vaporization critical point, are presented.

The development of atomic energy requires that the technologies for utilizing new coolants in reactor loops be perfected [1]. To create such technologies it is necessary to know the equation of state of the coolant in a wide temperature range, including the critical temperature. In recent years, the method of transmission of slow neutrons has been used in studies of the equation of state near the vaporization critical point for individual substances [2] and solutions [3, 4]. In this case, it is assumed that the total cross section for interaction of neutrons with molecules of the substance is independent of the temperature and does not have singularities at the point of the liquid–vapor phase transition. At the same time, experimental data indicating monotonic growth of the total cross section for the interaction of slow neutrons in some hydrogen-containing compounds with increasing temperature and the presence of a jump in the cross section at boiling points are presented in [5]. The purpose of this work is to study at different temperatures the cross section for the interaction of slow neutrons with a substance near its vaporization critical point.

The temperature dependence of the total cross section for the interaction of slow neutrons with a material can be obtained by determining the transmission of the neutrons by the material under study with mass m = const at different temperatures. In the slow neutron transmission method the well-known relation [6] between the intensity of the neutron before the sample I_0 and after the sample I is used:

$$I = I_0 \exp\{-N\sigma x\}. \quad (1)$$

The solution of this problem is complicated by the fact that near the critical point, because of the increase in the compressibility of the sample under the action of the gravitational field, there appears a characteristic distribution in the height distribution of the density – the gravitational effect [7]. Because of this the quantities N and I in formula (1) are functions of the height of the layer under study.

T. G. Shevchenko Kiev State University. Institute of the Chemistry of High Molecular Compounds, Academy of Sciences of the Ukrainian SSR, Kiev. Translated from Inzhenerno-Fizicheskii Zhurnal, Vol. 50, No. 5, pp. 760-763, May, 1986. Original article submitted February 28, 1985.

0022-0841/86/5005-0526$12.50